

Electrohydrodynamic instability in a horizontal fluid layer with electrical conductivity gradient subject to a weak shear flow

MIN-HSING CHANG¹, AN-CHENG RUO²
AND FALIN CHEN^{2†}

¹Department of Mechanical Engineering, Tatung University, Taipei 104, Taiwan

²Institute of Applied Mechanics, National Taiwan University, Taipei 106, Taiwan

(Received 10 September 2008 and in revised form 6 March 2009)

The stability of electrohydrodynamic flow between two horizontal plates with a vertical electrical conductivity gradient has been investigated in the presence of an imposed weak shear flow. The weak shear flow is driven by the horizontal pressure gradient, and the electrical conductivity gradient is generated by the concentration variation of the charge-carrying solute. An external electric field is applied across the fluid layer, and then the interaction between the unstable stratification of electrohydrodynamic flow and the shear arising from the plane Poiseuille flow is studied. A linear stability analysis has been implemented by considering both the longitudinal and transverse modes. Unlike the thermally stratified plane Poiseuille flow in which the longitudinal mode always dominates the onset of instability and is virtually unaffected by the superimposed shear flow, the instability of this mixed electrohydrodynamic–Poiseuille flow system is found to depend heavily on the shear flow, and the transverse mode may prevail over the longitudinal mode when the momentum of shear flow is sufficiently small. Particularly, an oscillatory longitudinal mode is found to exist, and it may become the critical mode when the conductivity gradient is small enough. The present results verify that an imposed weak shear flow may enhance the electrohydrodynamic instability in a fluid layer with electrical conductivity gradient.

1. Introduction

Electrohydrodynamic instability occurs in liquids with spatial gradients in the electrical properties. This subject has received much attention recently due to its widely promising applications in microfluidic devices (Storey 2005). In classical studies, these instability flows were discussed in systems either with abrupt changes in electrical properties (Taylor & McEwan 1965; Melcher & Taylor 1969; Michael & O'Neill 1970) or with spatial variations in electrical properties (Melcher & Firebaugh 1967; Turnbull & Melcher 1969; Hoburg & Melcher 1976; Hoburg & Melcher 1977; Hoburg 1977). The former is related to this study in comparable flow structure with an external applied electric field across the fluid layer, and the latter is similar in spatial gradient in electrical conductivity. Hence, here we will briefly introduce these studies.

Taylor & McEwan (1965) first considered the stability of the horizontal interface between conducting and non-conducting fluids under an applied uniform vertical

† Email address for correspondence: falin@iam.ntu.edu.tw

electric field. They found the interface becomes unstable and performed some experiments to verify their theoretical conclusions. Michael & O'Neill (1970) studied the stability of a layer of non-conducting fluid lying between two semi-infinite conducting fluids for both inviscid and viscous fluid models. Their results show that the criteria for instability are the same for both inviscid and viscous fluid cases. A detailed review for flows driven by interfacial electric stresses was given by Melcher & Taylor (1969). Recently, Thaokar & Kumaran (2005) investigated the stability of the interface between two dielectric fluids confined between parallel plates with a vertical electric field. They considered both perfect dielectric and leaky dielectric models and found that the interface becomes unstable when the applied potential exceeds a certain critical value which depends on the electrical properties of the fluids. Li *et al.* (2007) further analysed a problem similar to that of Thaokar & Kumaran (2005) but with the interface possessing surface charges and the existence of an electrical tangential shear stress there. They found the applied electric field always has a destabilizing effect for perfect dielectric model, but for the leaky dielectric model it may produce a destabilizing or stabilizing effect which also depends on the electrical properties of the two fluids.

For the electrohydrodynamic flows with spatial variations in electrical properties, Melcher & Firebaugh (1967) considered the case in which a slightly conducting liquid imposes a temperature gradient and a wave of electric field travels perpendicular to the temperature gradient. In this case, the temperature gradient results in a gradient in electrical conductivity, and they found the interaction between the conductivity gradient and the imposed electric field can pump the liquid. Turnbull & Melcher (1969) proposed a stability criterion for a perfectly insulating fluid with thermally induced gradients in density, permittivity and viscosity. They successfully performed an experiment to verify their theoretical criterion. Hoburg & Melcher (1976) studied the instability on the interface between two miscible fluids stressed by an equilibrium tangential electric field and with disparate electrical conductivities. They simulated the configuration by using a layer of exponentially varying conductivity and observed large-scale mixing of the fluids at relatively high electric fields. They further derived a bulk-coupled model to describe the linear instability mechanisms underlying the electrohydrodynamic mixing process associated with a diffusive conductivity gradient stressed by an orthogonal electric field (Hoburg & Melcher 1977). A related experimental and theoretical study has also been performed by Hoburg (1977). In contrast to the result of these studies that the electrical conductivity gradient is primarily induced by the thermal effect, Baygents & Baldessari (1998) considered the onset of electrohydrodynamic instability across a thin fluid layer with an electrical conductivity gradient which is associated with the concentration gradient of the charge-carrying solutes. They found the diffusion of conductivity is an important factor that results in a conditionally stable system. As they have discussed, such an electrohydrodynamic instability problem is of interest for electrically driven convection observed in spaceflight experiments on isoelectric focusing which is a separation process used to isolate and purify biological materials.

Based on the contributions of these studies, a subfield of electrohydrodynamics, named electrokinetics, has been extensively studied recently (Lin *et al.* 2004; Tardu 2004; Oddy & Santiago 2005; Chen *et al.* 2005; Storey 2005; Storey *et al.* 2005) due to its crucial applications in micro total analysis systems. The instability of electrokinetic flow involves the coupling of electrohydrodynamic and electro-osmotic flows. In particular, the models of electrohydrodynamic flow in these studies are basically developed from the model proposed by Baygents & Baldessari (1998). Although

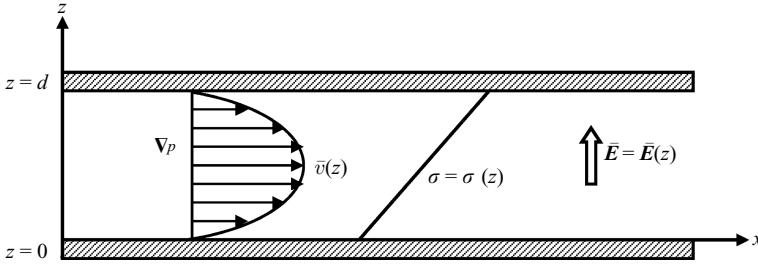


FIGURE 1. The system configuration.

electro-osmosis is usually used in microfluidic systems to manipulate the liquid flows, the fluid within microchannels also can be driven by an imposed pressure gradient (Stone, Stroock & Ajdari 2004). Accordingly, here we will consider the instability of electrohydrodynamic flow in a thin fluid layer coupled with a superimposed weak shear flow induced by a pressure gradient along the channel. The present theoretical model is primarily developed from the work of Baygents & Baldessari (1998), in which the electrical conductivity gradient varies linearly across the fluid layer and the diffusive processes of ionic solutes are taken into consideration. Furthermore, due to the presence of horizontal shear flow, the instability waves may align parallel with or vertical to the direction of shear flow. Therefore, both longitudinal and transverse modes will be investigated in this study. The results will benefit the further understanding of instability mechanisms for electrohydrodynamic flows in microfluidic systems.

2. Formulation of the problem

Consider the electrohydrodynamic motion in a layer of liquid occupying $z \in (0, d)$ between two parallel plates with a linear electrical conductivity gradient across the layer as shown in figure 1. A weak shear flow driven by the horizontal pressure gradient is superimposed on the fluid layer. The continuity and momentum equations can be expressed by

$$\nabla \cdot \mathbf{v} = 0, \quad (1)$$

$$\rho \left(\frac{\partial \mathbf{v}}{\partial t} + \mathbf{v} \cdot \nabla \mathbf{v} \right) = -\nabla p + \rho_f \mathbf{E} - \frac{1}{2} (\mathbf{E} \cdot \mathbf{E}) \nabla \varepsilon + \mu \nabla^2 \mathbf{v}, \quad (2)$$

where \mathbf{v} is the fluid velocity, ρ the density, p the pressure, ρ_f the free charge density, \mathbf{E} the applied electrical field, ε the dielectric constant and μ the dynamic viscosity. The second term on the right-hand side of (2) is the electrical body force induced by the action of the electric field on the free charge density in solution. The third term accounts for the electric force caused by the gradient of the dielectric constant, which is generally small and could be ignored. The free charge density ρ_f and the electrical field \mathbf{E} are coupled by the Gauss' law,

$$\nabla \cdot (\varepsilon \mathbf{E}) = \rho_f. \quad (3)$$

Moreover, the electrical current density \mathbf{J} for ohmic conductors is given by

$$\mathbf{J} = \sigma \mathbf{E} + \rho_f \mathbf{v}, \quad (4)$$

where σ is the electrical conductivity, and the conservation of charge yields

$$\frac{\partial \rho_f}{\partial t} + \nabla \cdot (\sigma \mathbf{E} + \rho_f \mathbf{v}) = 0. \quad (5)$$

Since the fluid layer is an ionic conductor, the conductivity varies with the local ion concentration. Accordingly, it has been shown by Melcher (1973) that the fluid conductivity could be described by

$$\frac{D\sigma}{Dt} = K_{eff} \nabla^2 \sigma, \quad (6)$$

where K_{eff} is the effective diffusivity of the ions due to Brownian motion. It is noted that (6) holds if the local charge accumulations relax rapidly in comparison with the viscous relaxation time and the time for ion electromigration (Baygents & Baldessari 1998).

Many experimental and theoretical studies have shown that a conductivity gradient may develop along the superimposed electric field in a thin fluid layer (Thormann, Mosher & Bier 1986; Mosher, Saville & Thormann 1992, pp. 163–230; Baygents & Baldessari 1998). As shown in figure 1, the conductivity varies linearly across the fluid layer, and thus it can be described by

$$\sigma(z) = \sigma_0 + \frac{\Delta\sigma}{d}z, \quad (7)$$

where $\Delta\sigma = \sigma_d - \sigma_0$, σ_0 and σ_d are respectively the electrical conductivity at $z = 0$ and $z = d$. Assume the superimposed horizontally weak shear flow will not disturb the steady conductivity profile between the parallel plates. As a result, we can derive the basic-state solution for this system as follows:

$$\bar{E}(z) = \frac{E_0 \mathbf{k}}{1 + (\Delta\sigma/\sigma_0)(z/d)}, \quad (8)$$

$$\bar{\rho}_f(z) = -\varepsilon \frac{\Delta\sigma/\sigma_0}{[1 + (\Delta\sigma/\sigma_0)(z/d)]^2} \frac{E_0}{d}, \quad (9)$$

$$\bar{\mathbf{v}}(z) = \frac{d^2}{2\mu} \frac{\partial p}{\partial x} \left(\frac{z^2}{d^2} - \frac{z}{d} \right) \mathbf{i}, \quad (10)$$

where E_0 is the electric-field strength at the bottom plate $z = 0$ and \mathbf{i} and \mathbf{k} are the unit vectors respectively in x - and z -direction. This solution indicates a constant current density flows through the fluid layer. To non-dimensionalize the governing equations, the following scales are used: length $\sim d$, velocity $\sim v_0$, time $\sim d/v_0$, pressure $\sim \rho v_0^2$, conductivity $\sim \Delta\sigma$, electric field E_0 and free charge density $\sim \varepsilon E_0 \Delta\sigma/d\sigma_0$. Here v_0 is the maximum velocity on the velocity profile defined by (10) and satisfying $v_0 = -(\partial p/\partial x)(d^2/8\mu)$. Accordingly, the dimensionless forms of governing equations (1), (2), (5) and (6) can be expressed as follows:

$$\nabla \cdot \mathbf{v} = 0, \quad (11)$$

$$\frac{D\mathbf{v}}{Dt} = -\nabla p + Q'(\nabla^2 \phi) \nabla \phi + \frac{1}{Re} \nabla^2 \mathbf{v}, \quad (12)$$

$$\frac{D}{Dt}(\nabla^2 \phi) = -\frac{\tau}{Re} \left\{ \left[1 + \frac{\Delta\sigma}{\sigma_0} \sigma \right] \nabla^2 \phi + \frac{\Delta\sigma}{\sigma_0} \nabla \sigma \cdot \nabla \phi \right\}, \quad (13)$$

$$\frac{D\sigma}{Dt} = \frac{1}{Sc_e Re} \nabla^2 \sigma. \quad (14)$$

Here we have used the dimensionless electric potential ϕ to describe both the electric field and free charge density in the forms

$$\mathbf{E} = -\nabla \phi, \quad (15)$$

$$\rho_f = -\frac{\sigma_0}{\Delta\sigma}\nabla^2\phi. \quad (16)$$

In (12)–(14), the parameters Q' , Re , τ and Sc_e are defined as

$$Q' = \frac{\varepsilon E_0^2}{\rho v_0^2}, \quad Re = \frac{v_0 d}{\nu}, \quad \tau = \frac{d^2 \sigma_0}{\nu \varepsilon}, \quad Sc_e = \frac{\nu}{K_{eff}}, \quad (17a-d)$$

where Q' represents the ratio of electrical and inertia forces; Re is the Reynolds number; τ represents the ratio of the viscous relaxation time to the charge relaxation time; Sc_e is the electric Schmidt number; and ν is the kinematic viscosity defined by $\nu = \mu/\rho$. The parameters Q' , Re and Sc_e are related by $Q' = Q/(Sc_e Re^2)$, in which $Q = \varepsilon E_0^2 d^2 / \mu K_{eff}$ represents the dimensionless electric-field strength or the scaled electric-energy density. The dimensionless forms of basic-state solution become

$$\bar{\sigma}(z) = z, \quad (18)$$

$$\bar{\mathbf{E}}(z) = \frac{1}{1 + (\Delta\sigma/\sigma_0)z} \mathbf{k}, \quad (19)$$

$$\bar{\rho}_f(z) = -\frac{1}{[1 + (\Delta\sigma/\sigma_0)z]^2}, \quad (20)$$

$$\bar{\mathbf{v}}(z) = 4(z - z^2)\mathbf{i}, \quad (21)$$

and accordingly the dimensionless electric potential ϕ can be derived as

$$\bar{\phi}(z) = \phi_0 - \frac{\sigma_0}{\Delta\sigma} \ln \left(1 + \frac{\Delta\sigma}{\sigma_0} z \right), \quad (22)$$

where ϕ_0 is the electric potential at $z = 0$. To perform a linear stability analysis for this flow, we superimposed a small disturbance on the basic-state solution as

$$\sigma(\mathbf{x}, t) = \bar{\sigma}(z) + \sigma'(\mathbf{x}, t), \quad (23)$$

with similar expressions for the other variables. Here the prime denotes the small perturbation variable. Following the usual procedures, we can obtain the small perturbation equations below:

$$\nabla \cdot \mathbf{v}' = 0, \quad (24)$$

$$\frac{\partial \mathbf{v}'}{\partial t} + \bar{v} \frac{\partial \mathbf{v}'}{\partial x} + w' \frac{d\bar{v}}{dz} \mathbf{i} = -\nabla p' + \frac{1}{Re} (\nabla^2 \mathbf{v}') + \frac{Q}{Sc_e Re^2} \left(\frac{d^2 \bar{\phi}}{dz^2} \nabla \phi' + \nabla^2 \phi' \frac{d\bar{\phi}}{dz} \mathbf{k} \right), \quad (25)$$

$$\begin{aligned} & \frac{\partial}{\partial t} (\nabla^2 \phi') + \bar{v} \left(\nabla^2 \frac{\partial \phi'}{\partial x} \right) + w' \frac{d^3 \bar{\phi}}{dz^3} \\ & = -\frac{\tau}{Re} \left\{ \left(1 + \frac{\Delta\sigma}{\sigma_0} \bar{\sigma} \right) \nabla^2 \phi' + \frac{\Delta\sigma}{\sigma_0} \left[\sigma' \frac{d^2 \bar{\phi}}{dz^2} + \frac{d\bar{\phi}}{dz} \frac{\partial \sigma'}{\partial z} + \frac{\partial \phi'}{\partial z} \frac{d\bar{\sigma}}{dz} \right] \right\}, \quad (26) \end{aligned}$$

$$\frac{\partial \sigma'}{\partial t} + \bar{v} \frac{\partial \sigma'}{\partial x} + w' \frac{d\bar{\sigma}}{dz} = \frac{1}{Sc_e Re} \nabla^2 \sigma'. \quad (27)$$

In order to eliminate the pressure term in (25), we take the double curl of this equation, and the z -component of the resulting equation yields

$$-\nabla^2 \frac{\partial w'}{\partial t} - \bar{v} \nabla^2 \frac{\partial w'}{\partial x} + \frac{d^2 \bar{v}}{dz^2} \frac{\partial w'}{\partial x} = \frac{1}{Re} [-\nabla^2 (\nabla^2 w')] + \frac{Q}{Sc_e Re^2} \left[\frac{d^3 \bar{\phi}}{dz^3} (\nabla_1^2 \phi') - \frac{d\bar{\phi}}{dz} (\nabla^2 \nabla_1^2 \phi') \right], \quad (28)$$

where ∇_1 is the operator defined as $\nabla_1 = \partial^2/\partial x^2 + \partial^2/\partial y^2$. Normal modes are then employed to decompose the disturbances in the form

$$\begin{Bmatrix} w'(\mathbf{x}, t) \\ \phi'(\mathbf{x}, t) \\ \sigma'(\mathbf{x}, t) \end{Bmatrix} = \begin{Bmatrix} \hat{w}(z) \\ \hat{\phi}(z) \\ \hat{\sigma}(z) \end{Bmatrix} f(x, y) e^{st}, \quad (29)$$

where $f(x, y) = \exp[i(\alpha_x x + \alpha_y y)]$ with $\alpha^2 = \alpha_x^2 + \alpha_y^2$. As a result, the governing equations can be written as

$$(s + 4i\alpha_x(z - z^2) - \frac{1}{Re}(D^2 - \alpha^2))(D^2 - \alpha^2)\hat{w} + 8i\alpha_x \hat{w} = -\frac{2\alpha^2 Q}{Sc_e Re^2} \left(\frac{\Delta\sigma}{\sigma_0}\right)^2 \times \frac{1}{[1 + (\Delta\sigma/\sigma_0)z]^3} \hat{\phi} + \frac{\alpha^2 Q}{Sc_e Re^2} \frac{1}{1 + (\Delta\sigma/\sigma_0)z} (D^2 - \alpha^2)\hat{\phi}, \quad (30)$$

$$\left\{ \left(s + \frac{\tau}{Re} \left(1 + \frac{\Delta\sigma}{\sigma_0} z \right) + 4i\alpha_x(z - z^2) \right) (D^2 - \alpha^2)\hat{\phi} + \frac{\tau}{Re} \frac{\Delta\sigma}{\sigma_0} D\hat{\phi} - 2 \left(\frac{\Delta\sigma}{\sigma_0} \right)^2 \times \frac{1}{[1 + (\Delta\sigma/\sigma_0)z]^3} \hat{w} = -\frac{\tau}{Re} \frac{\Delta\sigma}{\sigma_0} \left\{ \frac{\Delta\sigma}{\sigma_0} \frac{1}{[1 + (\Delta\sigma/\sigma_0)z]^2} \hat{\sigma} - \frac{1}{1 + (\Delta\sigma/\sigma_0)z} D\hat{\sigma} \right\}, \right. \quad (31)$$

$$\left(s - \frac{1}{Sc_e Re} (D^2 - \alpha^2) + 4i\alpha_x(z - z^2) \right) \hat{\sigma} = -\hat{w}, \quad (32)$$

where $D = d/dz$, $\alpha_x = \alpha \cos \phi_k$ and $\phi_k = \cos^{-1}(\alpha_x/\alpha)$ which is the angle between the wave propagation direction and the shear flow direction. The case of $\phi_k = 0$ indicates the axis of electrohydrodynamic convection roll is normal to the shear flow direction, which is called the transverse mode. On the other hand, the case of $\phi_k = \pi/2$ indicates the axis of convection roll is parallel to the shear flow direction, which is named the longitudinal mode. Note that the parameter τ for a thin fluid layer with charge-carrying solutes is generally quite large with the order of 10^7 (Baygents & Baldessari 1998). Therefore, it is reasonable to assume $\tau \rightarrow \infty$, and then (31) becomes

$$\left\{ \left(1 + \frac{\Delta\sigma}{\sigma_0} z \right) (D^2 - \alpha^2) + \frac{\Delta\sigma}{\sigma_0} D \right\} \hat{\phi} + \left\{ \left(\frac{\Delta\sigma}{\sigma_0} \right)^2 \frac{1}{[1 + (\Delta\sigma/\sigma_0)z]^2} - \left(\frac{\Delta\sigma}{\sigma_0} \right) \frac{1}{1 + (\Delta\sigma/\sigma_0)z} D \right\} \hat{\sigma} = 0. \quad (33)$$

The set of equations (30), (32) and (33) is solved together with rigid boundary conditions at $z = 0$ and $z = 1$ as follows:

$$\frac{d\hat{\phi}}{dz} = \hat{w} = \hat{\sigma} = \frac{d\hat{w}}{dz} = 0. \quad (34)$$

Here we assume the conductivity and the normal components of electric field and the velocity are fixed on the top and bottom rigid plates. Accordingly, a set of eighth-order eigenvalue problem is determined, which takes the form

$$F(s, \alpha, Q, Re, Sc_e, \Delta\sigma/\sigma_0, \phi_k) = 0. \quad (35)$$

This eigenvalue problem is solved by Chebyshev collocation method using Chebyshev polynomials as the set of basis functions. In general, 50 terms of the polynomials are sufficient to provide adequate resolution with economic consumption of computational cost. The linear instability boundary is indicated by the neutral curves on the plane of Q versus α . That is for given values of the other parameters, the neutral curves on the Q - α plane are used to determine the critical value of Q , Q_c , which represents the critical magnitude of the applied electric field needed to induce the electrically driven convection.

3. Results and discussion

This section is organized into three parts in order to provide full understanding of the stability characteristics for this problem. First, the electrohydrodynamic instability in a thin fluid layer without the imposed shear flow that had been studied by Baygents & Baldessari (1998) will be re-examined. Here we will focus on the instability behaviours under conditions with low electrical conductivity gradient and explore the possible existence of an oscillatory mode. Subsequently, the present electrohydrodynamic instability problem with the imposed weak shear flow between two rigid plates will be investigated, and the instability characteristics of the longitudinal and transverse modes will be discussed in details.

3.1. Stability characteristics without the superimposed shear flow

Baygents & Baldessari (1998) in their study simply assumed the exchange of stabilities holds to investigate the electrohydrodynamic instability behaviours in a thin fluid layer with an electrical conductivity gradient. Both stress-free and rigid boundary conditions are considered in their numerical results. Although their theoretical model can successfully characterize the electrically driven convection in an initially quiescent fluid layer, they also found that the numerical scheme will lose the accuracy requirements, since the loop of neutral curve will rise and recede rapidly to the small wavenumber region, as the electrical conductivity gradient is less than a certain critical value, for example 4.01, for the case of stress-free boundaries. Accordingly, they suggested that the fluid layer is only sensitive to long-wavelength disturbances and that the lateral boundaries will exert a substantial stabilizing influence when the electrical conductivity gradient is small. However, a fluid layer of infinite extent is assumed without lateral boundaries in their model. Such a conclusion is indeed questionable. From the physical point of view, it is also suspicious that the fluid layer will always be stable even though the strength of applied electric field approaches infinity. Therefore, in this study we take the overstability into consideration and perform a more complete linear stability analysis to examine the possible existence of an oscillatory mode in this electrically driven convection system.

To accomplish the analysis, the dimensionless governing equations are derived by employing the same scales as those adopted by Baygents & Baldessari (1998): length $\sim d$, velocity $\sim \sqrt{\varepsilon E_0^2 \Delta\sigma / \rho\sigma_0}$, time $\sim \sqrt{d^2 \rho\sigma_0 / \varepsilon E_0^2 \Delta\sigma}$, pressure $\sim \varepsilon E_0^2 \Delta\sigma / \sigma_0$, conductivity $\sim \Delta\sigma$, electric field $\sim E_0$ and free charge density $\sim \varepsilon E_0 \Delta\sigma / d\sigma_0$. Note that the scales of velocity, time and pressure are different from those used in the present

study with an imposed weak shear flow. Since a quiescent basic state is assumed in Baygents & Baldessari (1998), the velocity scale is given by the balance of inertia and electrical forces, and accordingly the time and pressure scales are determined. Moreover, the basic-state solution of velocity is zero which is also different from the present case given by (21). Following the similar procedures of Baygents & Baldessari (1998) while holding the growth rate constant in the resultant of linear stability equations, we have

$$\frac{2(\Delta\sigma/\sigma_0)^{1/2}}{\tau} \left(\frac{Q}{Sc_e}\right)^{1/2} \frac{(\Delta\sigma/\sigma_0)^2}{[1+(\Delta\sigma/\sigma_0)z]^3} \hat{w} + \frac{\Delta\sigma/\sigma_0}{[1+(\Delta\sigma/\sigma_0)z]} D\hat{\sigma} - \frac{(\Delta\sigma/\sigma_0)^2}{[1+(\Delta\sigma/\sigma_0)z]^2} \hat{\sigma} - \left(1 + \frac{\Delta\sigma}{\sigma_0} z\right) (D^2 - \alpha^2)\hat{\phi} - \frac{\Delta\sigma}{\sigma_0} D\hat{\phi} = s \frac{(\Delta\sigma/\sigma_0)^{1/2}}{\tau} \left(\frac{Q}{Sc_e}\right)^{1/2} (D^2 - \alpha^2)\hat{\phi}, \quad (36)$$

$$(D^2 - \alpha^2)\hat{\sigma} - \left(\frac{\Delta\sigma}{\sigma_0}\right)^{1/2} (QSc_e)^{1/2} \hat{w} = s \left(\frac{\Delta\sigma}{\sigma_0}\right)^{1/2} (QSc_e)^{1/2} \hat{\sigma}, \quad (37)$$

$$\frac{\alpha^2}{(\Delta\sigma/\sigma_0)[1+(\Delta\sigma/\sigma_0)z]} (D^2 - \alpha^2)\hat{\phi} - \frac{2\alpha^2(\Delta\sigma/\sigma_0)}{[1+(\Delta\sigma/\sigma_0)z]^3} \hat{\phi} + \left(\frac{\Delta\sigma}{\sigma_0}\right)^{-1/2} \left(\frac{Q}{Sc_e}\right)^{-1/2} (D^2 - \alpha^2)^2 \hat{w} = s(D^2 - \alpha^2)\hat{w}, \quad (38)$$

The above set of equations (36)–(38) is then solved together with stress-free boundary conditions at $z = 0$ and $z = 1$,

$$\frac{d\hat{\phi}}{dz} = \hat{w} = \hat{\sigma} = \frac{d^2\hat{w}}{dz^2} = 0, \quad (39)$$

or with the same rigid boundary conditions as (34).

The numerical results are first compared with those of Baygents & Baldessari (1998) for the stationary mode. It is found that the present study can reproduce their results exactly. For example, as seen in figures 2(*d*) and 3(*d*), the lower branch of the stationary mode indicated by the solid curve is the same as the corresponding curve in Baygents & Baldessari (1998). In figure 4(*a*) the solid curve for the case with stress-free boundaries is also identical to the curve in figure 11 in their study. In the following paragraphs, we will elucidate the existence of the oscillatory mode in cases with either stress-free or rigid boundary conditions by showing the variations of neutral curves to provide a thorough understanding of the instability characteristics of this electrohydrodynamic flow system.

The neutral curves for the case with stress-free boundaries are shown in figures 2(*a*)–2(*d*) for four typical conductivity gradients with $Sc_e = 10^3$. As demonstrated in figure 2(*a*), the neutral curve of the oscillatory mode is found to exist and dominate the onset of instability when the conductivity gradient is small enough. The corresponding magnitude of the oscillatory frequency $|s_i|$ is also shown in the figure. As we have discussed, in the study of Baygents & Baldessari (1998) they failed to find the linear instability boundary when the conductivity gradient is less than 4.01 in the case of stress-free boundaries. The present results show that their assumption regarding the applicability of exchange of stabilities is incorrect. Actually, the oscillatory mode plays an important role in the instability behaviours, especially in the conditions with a small electrical conductivity gradient. As the conductivity gradient increases slightly to 4.1, a small loop of neutral curve of the stationary mode begins to appear in the

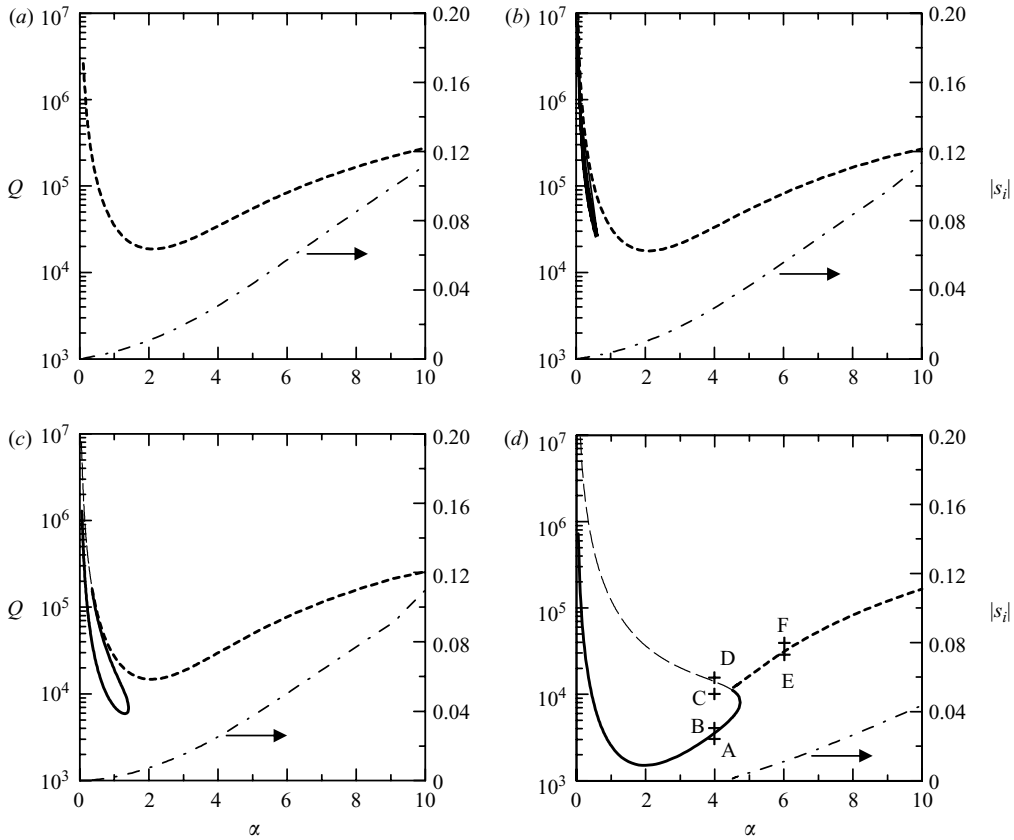


FIGURE 2. Neutral curves for stress-free boundary conditions with $Sc_e = 1000$: (a) $\Delta\sigma/\sigma_0 = 4$; (b) $\Delta\sigma/\sigma_0 = 4.1$; (c) $\Delta\sigma/\sigma_0 = 4.5$; and (d) $\Delta\sigma/\sigma_0 = 10$. The dashed line is the oscillatory mode, and the solid line is the stationary mode. Note that the upper dashed lines in the left loops for the stationary mode in (c) and (d) means the neutral state is determined by the second leading eigenvalue. The dash-dotted lines indicate the corresponding oscillatory frequency of the oscillatory mode referring to the right vertical scale.

low-wavenumber region, which means the instability of the stationary mode will be initiated with an increase of the conductivity gradient as shown in figure 2(b). The neutral curve of the oscillatory mode will dip lower gradually, while the loop of the stationary mode will extend and descend more rapidly than the oscillatory mode with increasing conductivity gradient as evidenced in figure 2(c). This result suggests that the critical mode at the onset of instability will shift to the stationary mode when the conductivity gradient exceeds a certain critical value, which is about 4.3 in this case. Finally, as shown in figure 2(d), the lower branch of the stationary mode becomes dominant, and the local minimum on the branch of the oscillatory mode disappears. Note that the neutral curves of the stationary mode in figures 2(c) and 2(d) are separated into two branches: the lower branch and the upper branch. On the lower branch indicated by the solid line, the neutral state is determined by the leading eigenvalue of the spectra of growth rate s , while on the upper branch indicated by dashed line, the neutral state is determined by the second leading eigenvalue. For the branch of the oscillatory mode, it is the same as the lower branch of the stationary mode, which is determined by the first leading eigenvalue. In order to interpret the

Point	α	Q	s_r	s_i
A	4	3×10^3	-0.00070204	0
			-0.00871883	0
B	4	4×10^3	0.00045324	0
			-0.00715735	0
C	4	10^4	0.00340950	0
			-0.00251533	0
D	4	1.5×10^4	0.00329627	0
			0.00080892	0
E	6	3×10^4	-0.00017092	0.01071536
			-0.00017092	-0.01071536
F	6	4×10^4	0.00122196	0.01369494
			0.00122196	-0.01369494

TABLE 1. The first two leading eigenvalues of selected points in figure 2(d) with stress-free boundary conditions.

variations of the leading eigenvalues of s , we choose six typical points A–F in figure 2(d) and give the first two leading eigenvalues on each point in table 1. One can see that for an assigned wavenumber $\alpha = 4$, the real part s_r of the first leading eigenvalue will switch from negative at point A to positive at point B, which means there exists a neutral point between A and B with $s_r = s_i = 0$. Similar phenomena can be observed for the second leading eigenvalues of points C and D, though the first leading eigenvalue is still the mode with the highest positive growth rate. At the points E and F with $\alpha = 6$, it is found that the first two leading eigenvalues are a pair of conjugate complex, and the real part s_r will change sign from negative at point E to positive at point F, which implies an oscillatory neutral state exists between them.

Similar results for the case with rigid boundary conditions are demonstrated in figures 3(a)–3(d) for four assigned conductivity gradients. Apparently, rigid boundaries exert a stabilizing effect on this electrohydrodynamic flow, since the neutral curves rise significantly compared to the case of stress-free boundaries under the same conductivity gradient. The instability is still dominated by the oscillatory mode at $\Delta\sigma/\sigma_0 = 7$ as shown in figure 3(a), and the branch of the stationary mode appears gradually as the conductivity gradient increases, for example, as illustrated in figure 3(b) at $\Delta\sigma/\sigma_0 = 14$. Obviously, rigid boundaries extend the range of the conductivity gradient in which the oscillatory mode predominates over the stationary mode. As the conductivity gradient increases further, the branch of the stationary mode declines rapidly and then dominates the onset of instability eventually as indicated in figures 3(c)–3(d). The variations of the first two leading growth rates are given in table 2 for the six typical points G–L in figure 3(d). The variational characteristics are the same as those in table 1 for the case of stress-free boundaries.

Figures 4(a) and 4(b) illustrate the variations of the critical electric-field number Q_c and critical wavenumber α_c with the conductivity gradient, respectively. Apparently, rigid boundaries stabilize the fluid layer, since a higher electric field is required

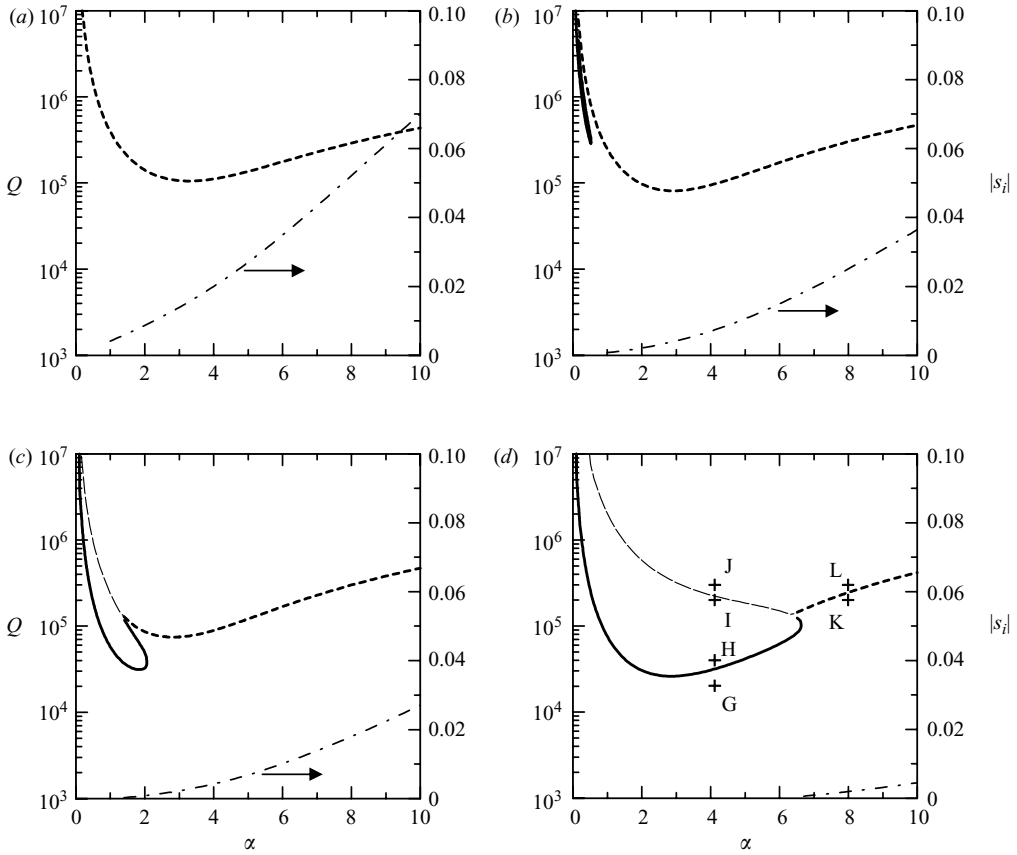


FIGURE 3. Neutral curves for rigid boundary conditions with $Sc_e = 1000$: (a) $\Delta\sigma/\sigma_0 = 7$; (b) $\Delta\sigma/\sigma_0 = 14$; (c) $\Delta\sigma/\sigma_0 = 18$; (d) $\Delta\sigma/\sigma_0 = 50$. The definition of each curve is the same as in figure 2.

to trigger the onset of instability for an assigned conductivity gradient. As shown in figure 4(a), the value of Q_c decreases gradually with the conductivity gradient for the oscillatory modes in both cases, indicating the conductivity gradient is a destabilizing factor for the oscillatory mode, while after the shift of critical mode to the stationary mode, a minimum appears on each curve, and then Q_c increases monotonically with $\Delta\sigma/\sigma_0$. To interpret such a variational relationship, it is necessary to consider the basic physical mechanisms affecting the onset of electrohydrodynamic instability. The instability of fluid motion in this system is mainly dominated by the dielectrophoretic effect, the diffusion of ionic solutes and the fluid viscosity. When a parcel of fluid within the fluid layer moves upward due to the action of electric field, it enters a region with higher conductivity and lower electric field. And if a parcel of low conductivity fluid is surrounded by higher conductivity fluid, it tends to move towards region with low electric field. This motion is referred to as the dielectrophoretic effect which is induced by the gradient of electric field. This effect intends to drive an upward fluid motion continuously. On the other hand, the diffusion of ionic solutes tends to impede the onset of electrohydrodynamic motion and thus produces a stabilizing effect on the fluid layer. If the diffusive effect is large enough, the upward fluid motion will be inhibited, since the diffusion of charge-carrying solutes

Case	α	Q	s_r	s_i
G	4	2×10^4	-0.00030961 -0.00155463	0 0
H	4	4×10^4	0.00019454 -0.00100744	0 0
I	4	2×10^5	0.00162590 -0.00010068	0 0
J	4	3×10^5	0.00207535 0.00024084	0 0
K	8	2×10^5	-0.00026663 -0.00026663	0.00149279 -0.00149279
L	8	3×10^5	0.00030270 0.00030270	0.00240450 -0.00240450

TABLE 2. The first two leading eigenvalues of selected points in figure 3(d) with rigid boundary conditions.

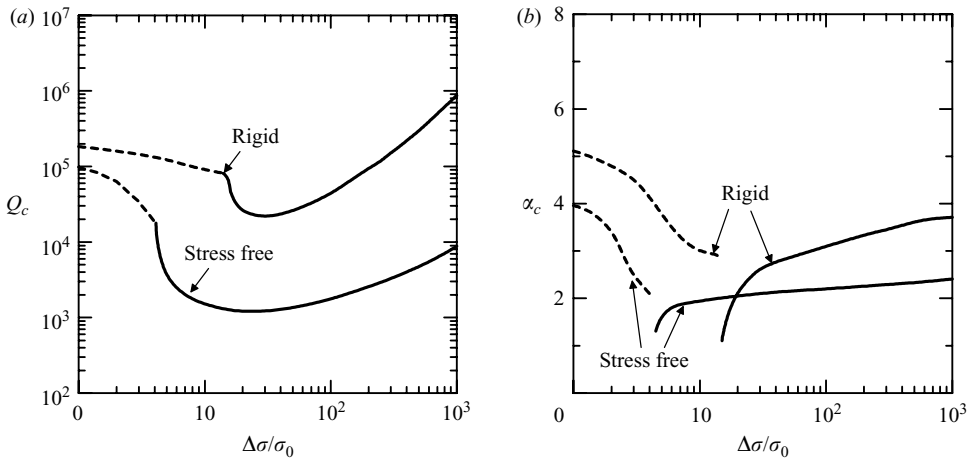


FIGURE 4. The variations of (a) Q_c and (b) α_c with conductivity gradient $\Delta\sigma/\sigma_0$ at $Sc_e = 1000$. The dashed and solid lines represent the critical mode determined by the oscillatory mode and the stationary mode, respectively. The shift from the oscillatory mode to the stationary mode occurs respectively at $\Delta\sigma/\sigma_0 = 4.15$ and $\Delta\sigma/\sigma_0 = 14.9$ for stress-free and rigid boundary conditions.

tends to remove the conductivity difference between the upwardly flowing fluid parcel and its surroundings, and thus the dielectrophoretic driving force is balanced by the elimination of conductivity difference. The fluid viscosity will also resist the upward fluid motion. However, as the conductivity gradient is small, the diffusive effect is insignificant, and the dielectrophoretic effect will be enhanced with increasing $\Delta\sigma/\sigma_0$, since the conductivity difference between the upward-moving fluid parcel and its surroundings will increase. Consequently, the fluid layer tends to be destabilized by an increase of $\Delta\sigma/\sigma_0$ in the region of small conductivity gradient. Particularly, once

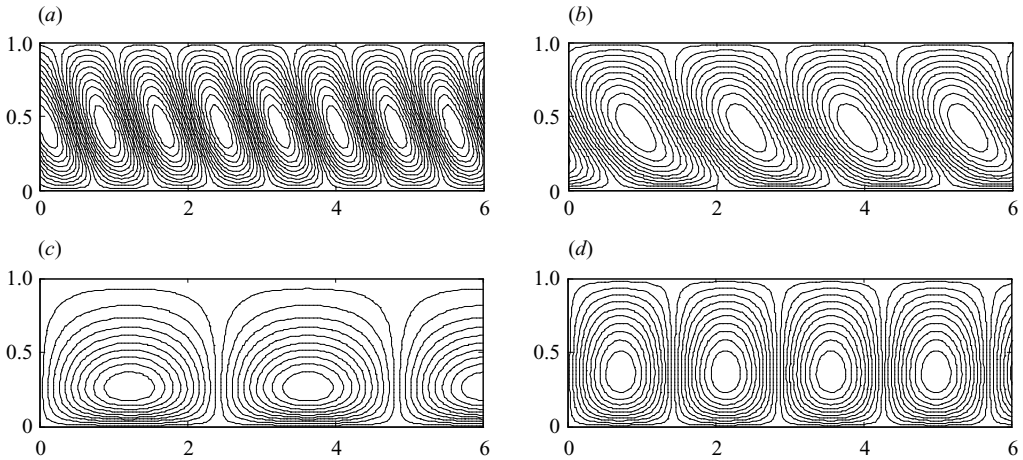


FIGURE 5. Convection cell patterns for four typical critical states with stress-free boundary conditions at $Sc_e = 1000$: (a) $\Delta\sigma/\sigma_0 = 1$, $\alpha_c = 3.96$, $Q_c = 9.794 \times 10^4$, $(s_r, s_i) = (0, 0.113)$; (b) $\Delta\sigma/\sigma_0 = 4.1$, $\alpha_c = 2.10$, $Q_c = 1.779 \times 10^4$, $(s_r, s_i) = (0, 1.075 \times 10^{-2})$; (c) $\Delta\sigma/\sigma_0 = 4.5$, $\alpha_c = 1.31$, $Q_c = 5.936 \times 10^3$, $(s_r, s_i) = (0, 0)$; and (d) $\Delta\sigma/\sigma_0 = 100$, $\alpha_c = 2.21$, $Q_c = 1.776 \times 10^3$, $(s_r, s_i) = (0, 0)$.

the onset of instability is primarily dominated by the dielectrophoretic effect, the instability mode tends to be the oscillatory mode in the form of travelling wave rather than the stationary mode. As the value of $\Delta\sigma/\sigma_0$ increases further, the diffusive effect becomes pronounced gradually and makes the critical mode switch to the stationary mode, though the dielectrophoretic effect still predominates and continues to destabilize the fluid layer until the value of Q_c reaches a minimum. After that, the diffusive transport is comparatively strong enough to resist the upward fluid motion, and thus a higher value of Q_c is necessary to trigger the occurrence of instability.

By the profiles of $\bar{E}d\bar{E}/dz$, which indicate the electric body force acting on the volume charge, Baygents & Baldessari (1998) have pointed out that the portion of fluid in which the dielectrophoretic forces are significant is close to lower-conductivity boundary and becomes increasingly narrow as the conductivity gradient increases. Therefore, they suggested that the lower boundary will produce a strong stabilizing effect at high values of $\Delta\sigma/\sigma_0$. The results as shown in figure 4(b) reveal that rigid boundaries generally seem to restrict the convective motion and shorten the wavelength of the critical mode under the same conductivity gradient in comparison to the case of stress-free boundaries. The discontinuities in both cases are due to the shift of critical mode from the oscillatory to the stationary mode.

The onset of electrohydrodynamic instability is further characterized by examining the flow patterns corresponding to the different instability modes. In the case of stress-free boundaries, four typical flow patterns at the critical states with $\Delta\sigma/\sigma_0 = 1$, 4.1, 4.5 and 100 are shown in figures 5(a)–5(d), respectively. The critical oscillatory mode at $\Delta\sigma/\sigma_0 = 1$ as shown in figure 5(a) appears to be an inclined convection cell propagating in the horizontal direction. Since the dielectrophoretic effect is significant, and the diffusive effect could be ignored, the convection cell almost occupies the whole thickness of the fluid layer, and the centre of convection cell is quite close to the midline. The enhancement of dielectrophoretic effect makes the oscillatory convection cell extend gradually, while the centre of convection cell descends slowly

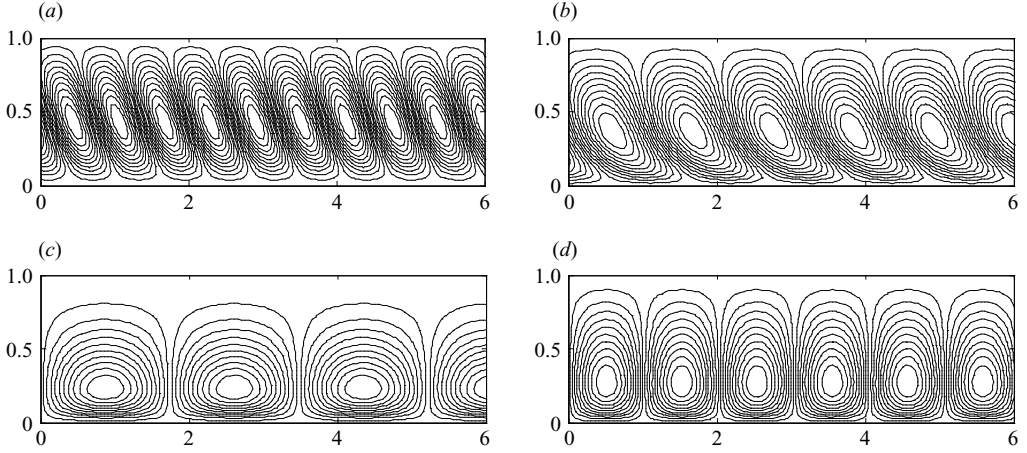


FIGURE 6. Convection cell patterns for four typical critical states with rigid boundary conditions at $Sc_e = 1000$: (a) $\Delta\sigma/\sigma_0 = 1$, $\alpha_c = 5.15$, $Q_c = 1.831 \times 10^5$, $(s_r, s_i) = (0, 0.124)$; (b) $\Delta\sigma/\sigma_0 = 14$, $\alpha_c = 2.92$, $Q_c = 8.124 \times 10^4$, $(s_r, s_i) = (0, 0.004)$; (c) $\Delta\sigma/\sigma_0 = 18$, $\alpha_c = 1.81$, $Q_c = 3.136 \times 10^4$, $(s_r, s_i) = (0, 0)$; and (d) $\Delta\sigma/\sigma_0 = 100$, $\alpha_c = 3.12$, $Q_c = 4.424 \times 10^4$, $(s_r, s_i) = (0, 0)$.

with increasing $\Delta\sigma/\sigma_0$ as shown in figure 5(b). When the stationary mode begins to dominate the critical mode, the influence of diffusive transport grows gradually, and the convection is mostly within the lower half of the fluid layer, especially in the region adjacent to the lower boundary. As $\Delta\sigma/\sigma_0$ increases further and far away from the state of minimum Q_c , it requires higher electric field to raise the dielectrophoretic force and overcome the pronounced stabilizing effect due to diffusive transport. Therefore, as demonstrated in figure 5(d), the wavelength will be shortened, and the centre of convection cell will rise again. The convection still occupies the whole fluid layer, and it is much stronger in the region near the lower-conductivity boundary. Figures 6(a)–6(d) illustrate the flow patterns for the case of rigid boundaries with $\Delta\sigma/\sigma_0 = 1$, 14, 18 and 100, respectively. The variation of flow patterns is similar to that in the case with stress-free boundaries. However, it is obvious that rigid boundaries indeed constrain the development of convection cells. As seen in these figures, the upper rigid boundary appears to restrict the upward fluid motion driven by the dielectrophoretic force. As a result, the convection cells move closer to the lower boundary and cause weaker convection in the region near the upper boundary in contrast to the case with stress-free boundaries.

3.2. Stability characteristics of longitudinal modes

The longitudinal mode means the axes of convection cells are parallel to the superimposed weak shear flow. Before we proceed to discuss its instability behaviours, it should be reminded that in this section and §3.3 we consider the case with rigid boundaries only as the eigenvalue problem defined by (35). Figure 7(a) illustrates the neutral curves at $Re = 1$ for several typical values of $\Delta\sigma/\sigma_0$, and the corresponding oscillatory frequencies of the oscillatory longitudinal modes are shown in figure 7(b). It is found that the neutral curves are the same as those obtained from the case without the superimposed shear flow. Actually, the neutral curves are independent of the Reynolds number, indicating the presence of a weak shear flow will not affect the stability of the longitudinal mode. Such an instability characteristic is the same as that of the Rayleigh–Bénard–Poiseuille (RBP) flow system in which the longitudinal mode

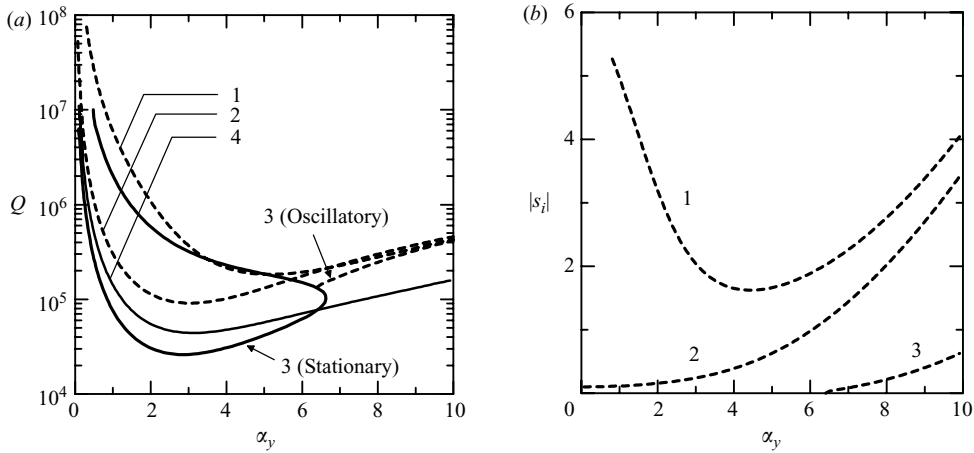


FIGURE 7. (a) The neutral curves and (b) the corresponding oscillatory frequency $|s_i|$ of the longitudinal mode at $Re=1$ and $Sc_e=1000$. The dashed and solid curves in (a) represent the oscillatory and the stationary mode, respectively: (1) $\Delta\sigma/\sigma_0=1$; (2) $\Delta\sigma/\sigma_0=10$; (3) $\Delta\sigma/\sigma_0=50$; and (4) $\Delta\sigma/\sigma_0=100$.

is also not affected by the horizontal Poiseuille flow (Clever & Busse 1992; Carriere & Monkewitz 1999). Especially in the RBP system the longitudinal mode always appears to be the most unstable mode with an invariable critical Rayleigh number. The transverse mode has the same instability as the longitudinal mode only when the Reynolds number of the shear flow approaches zero. As the strength of shear flow will increase, the critical Rayleigh number of the transverse mode will increase monotonically. Thus, the transverse mode never becomes dominant in the RBP system with an infinitely extended fluid layer. However, in the present electrohydrodynamic–Poiseuille flow system, the interaction between the instability mechanisms is more complicated, and it is found that the transverse mode may dominate the onset of instability when the fluid layer is subject to a weak shear flow. The details will be demonstrated in the next section. Furthermore, the oscillatory longitudinal mode has never been found in the RBP system, while in the present system the oscillatory longitudinal modes are found to exist and may determine the critical mode at the onset of instability. The results in figure 7(b) show that the oscillatory frequency of the longitudinal mode will decrease gradually with increasing conductivity gradient. Once the critical mode shifts from the oscillatory mode to the stationary mode, the corresponding oscillatory frequency drops to zero.

The influence of the electric Schmidt number on the longitudinal mode is also worth noting. The results are shown in figure 8 for four typical values of Sc_e . Obviously, the minimum on the neutral curve is independent of the value of Sc_e if Sc_e is greater than 10^3 . That is according to the definition of Sc_e in (17d), if the fluid viscosity is much greater than the effective diffusivity of ions, the variation of Sc_e will play no role in the factors affecting the critical value Q_c of the longitudinal mode, while if Sc_e reduces to the order of 10^2 , which implies relatively smaller strength of viscosity, the longitudinal mode will be slightly more unstable due to the reduction of the resistance of viscosity. Since the onset of instability is an oscillatory longitudinal mode at $\Delta\sigma/\sigma_0=10$, the corresponding oscillatory frequency for each case in figure 8(a) is shown in figure 8(b). One can see that the value of $|s_i|$ is quite sensitive to the variation of Sc_e . Although the neutral curve seems to be invariable as $Sc_e > 10^3$, the

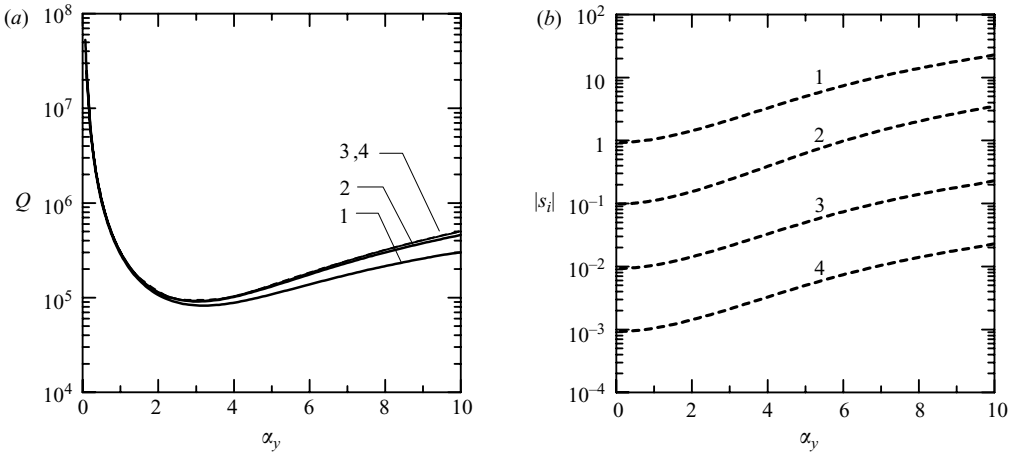


FIGURE 8. (a) The neutral curves and (b) the corresponding oscillatory frequency $|s_i|$ of the longitudinal mode at $Re = 1$ and $\Delta\sigma/\sigma_0=10$: (1) $Sc_e = 10^2$; (2) $Sc_e = 10^3$; (3) $Sc_e = 10^4$; and (4) $Sc_e = 10^5$.

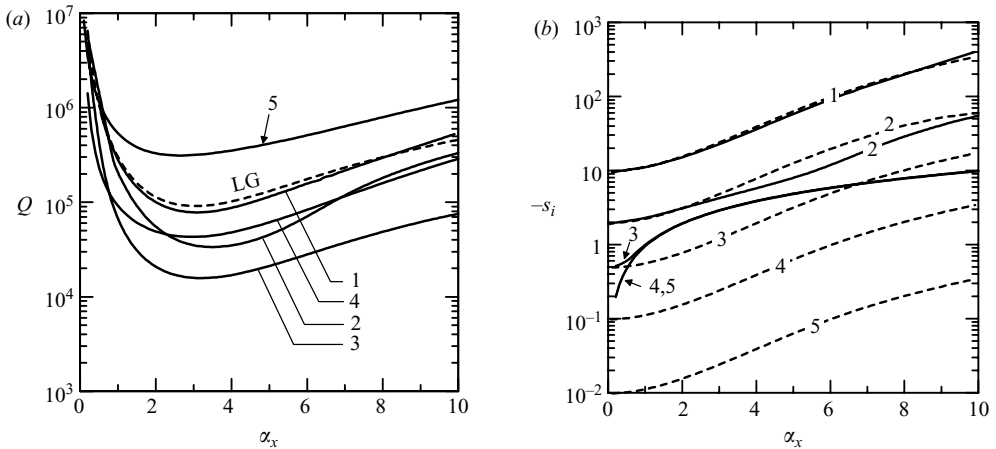


FIGURE 9. (a) The neutral curves and (b) the corresponding oscillatory frequency ($-s_i$) of the transverse mode at $Sc_e = 1000$ and $\Delta\sigma/\sigma_0 = 10$: (1) $Re = 0.01$; (2) $Re = 0.05$; (3) $Re = 0.2$; (4) $Re = 1$; and (5) $Re = 10$. The results of the longitudinal mode (LG) are given here by the dashed lines for comparison.

oscillatory frequency is found to be inversely proportional to Sc_e , and the curve in figure 7(b) appears to move parallel to the lower position with one order of reduction in $|s_i|$ if the value of Sc_e has one order of increase.

3.3. Stability characteristics of transverse modes

In contrast to the longitudinal mode, the convection cells of the transverse mode are aligned along the weak shear flow and with their axes normal to the shear flow direction. The superimposed weak shear flow is represented by the Reynolds number, and its effects on the neutral curves of the transverse mode are demonstrated in figure 9 for several typical values of Re with $Sc_e = 10^3$ and $\Delta\sigma/\sigma_0 = 10$. As shown in figure 9(a), it is found that the neutral curve of the transverse mode tends to be

the same as the longitudinal mode as the Reynolds number approaches zero, while as the Reynolds number increases, the neutral curve of the transverse mode will dip lower gradually till about $Re = 0.2$ and then rise rapidly. Finally, the longitudinal mode becomes the critical mode again when Re exceeds a certain critical value. The corresponding oscillatory frequency of each curve is shown in figure 9(b). The vertical axis is expressed in terms of $(-s_i)$, since s_i is negative for the transverse modes, which indicates the travelling wave will propagate in the direction of shear flow with a dimensionless velocity defined by $(-s_i/\alpha_x)$. Obviously, the magnitude of $(-s_i)$ for the transverse mode decreases quickly with Re and then appears to be invariable, as Re is greater than 1. In contrast to the results of transverse modes, the longitudinal modes have the same variational behaviour of $(-s_i)$ in each case of Re , and its value is inversely proportional to Re for any assigned wavenumber α_x . This result does not mean that the variation of Re will affect the instability behaviour of the longitudinal mode. Actually, since the scale to non-dimensionalize the oscillatory frequency is v_0/d , it is evident that the dimensionless oscillatory frequency $(-s_i)$ will be inversely proportional to the Reynolds number due to the constant dimensional oscillatory frequency.

As we have discussed in the previous section, such an instability characteristic is quite different from that of the famous RBP system. The present results show that the transverse mode may prevail over the longitudinal mode when the system is under the action of a horizontally weak shear flow. The main reason may be interpreted from the interaction between the instability mechanisms in this electrohydrodynamic–Poiseuille flow system. When the Reynolds number increases from zero, the imposed weak shear flow will enhance the upward electrohydrodynamic motion more than the diffusive effect and thus destabilize the fluid layer in the form of travelling wave along the shear flow direction. Simultaneously, the effect of diffusive transport also grows gradually with increasing Re . Once this effect is sufficiently strong, the neutral curve of the transverse mode cease to descend and start to rise with further increase in Re . As a result, the longitudinal mode eventually dominates the onset of instability, since the neutral curve of the transverse mode rises above that of the longitudinal mode if the Reynolds number is large sufficiently. The cell patterns of the four selected cases at critical state with $Re = 0.05, 0.2, 1$ and 10 are shown in figures 10(a)–10(d), respectively. As seen in figure 10(a), the transverse mode appears to be an inclined travelling wave in the horizontal direction. When Re increases to 0.2 as shown in figure 10(b), the inclined angle of the convection cell decreases, and the convection strength in the upper half-channel reduces significantly, especially in the region near the top plate, which is caused by the conspicuous enhancement of diffusive effect due to the imposed weak shear flow. This phenomenon continues with increasing Re as shown in figure 10(c) for $Re = 1$, and the wavelength also increases gradually. As Re increases further, the convection cells are gradually distorted, especially in the centre due to the action of the imposed shear flow as shown in figure 10(d). However, such a transverse travelling wave will not become critical, since the critical value of Q_c is higher than that of the longitudinal mode under this condition with $Re = 10$.

The effect of conductivity gradient on the neutral curve of the transverse mode is illustrated in figure 11(a), and the corresponding oscillatory frequency is given in figure 11(b). It is found that the instability behaviour is similar to that of the longitudinal mode, in which the minimum of Q on the neutral curve will first decrease with $\Delta\sigma/\sigma_0$, reach a minimum and then increase rapidly. In comparison with the results shown in figure 7, the effect of the conductivity gradient on the transverse mode is obviously more significant than that on the longitudinal mode when the value of $\Delta\sigma/\sigma_0$ is small,

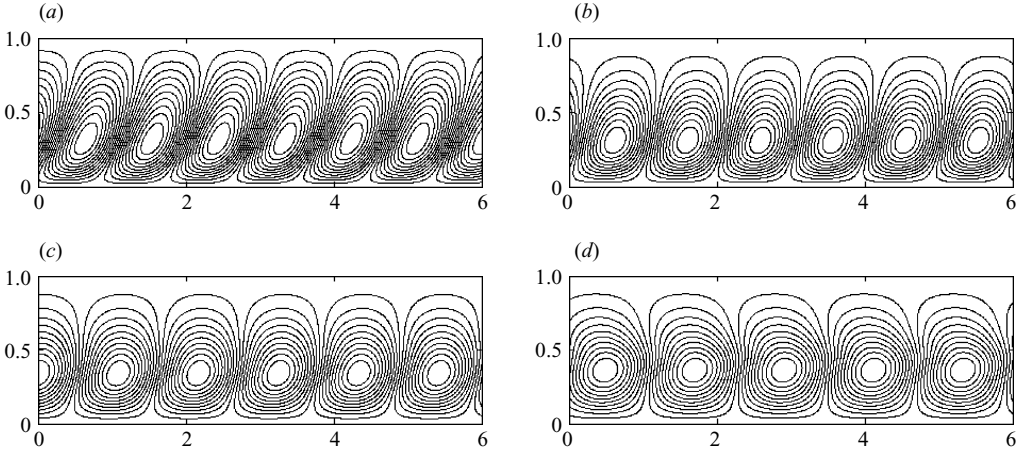


FIGURE 10. Convection cell patterns of the transverse mode for four typical critical state with $Sc_e = 1000$ and $\Delta\sigma/\sigma_0 = 10$: (a) $Re = 0.05$, $\alpha_x = 3.50$, $Q_c = 3.359 \times 10^4$, $(s_r, s_i) = (0, -4.937)$; (b) $Re = 0.2$, $\alpha_x = 3.20$, $Q_c = 1.574 \times 10^4$, $(s_r, s_i) = (0, -3.068)$; (c) $Re = 1$, $\alpha_x = 2.95$, $Q_c = 4.295 \times 10^4$, $(s_r, s_i) = (0, -2.850)$; (d) $Re = 10$, $\alpha_x = 2.64$, $Q_c = 3.123 \times 10^5$, $(s_r, s_i) = (0, -2.593)$.

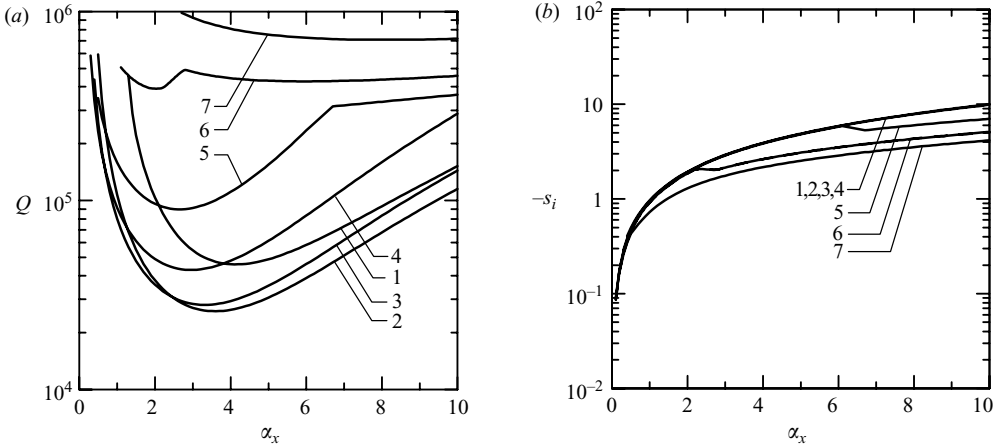


FIGURE 11. (a) The neutral curves and (b) the corresponding oscillatory frequency ($-s_i$) of the transverse mode at $Sc_e = 1000$ and $Re = 1$: (1) $\Delta\sigma/\sigma_0 = 1$; (2) $\Delta\sigma/\sigma_0 = 3$; (3) $\Delta\sigma/\sigma_0 = 5$; (4) $\Delta\sigma/\sigma_0 = 10$; (5) $\Delta\sigma/\sigma_0 = 20$; (6) $\Delta\sigma/\sigma_0 = 50$; and (7) $\Delta\sigma/\sigma_0 = 100$.

since the neutral curve of the transverse mode dips lower than that of the longitudinal mode under the same value of $\Delta\sigma/\sigma_0$. But the neutral curve of the transverse mode soon begins to rise after the case of $\Delta\sigma/\sigma_0 = 3$. At $\Delta\sigma/\sigma_0 = 20$, the minimum on the neutral curve is greater than that of the longitudinal mode, which means the instability will be dominated by the longitudinal mode again once the conductivity gradient is large enough. Note that the neutral curve gradually appears to have a bimodal phenomenon as shown in the case of $\Delta\sigma/\sigma_0 = 50$. That is two local minima can be observed on the neutral curve. However, this phenomenon is insignificant, since it always occurs when the neutral curve is much higher than that of the longitudinal mode. Figures 12(a)–12(d) show the convection cell patterns for four typical cases

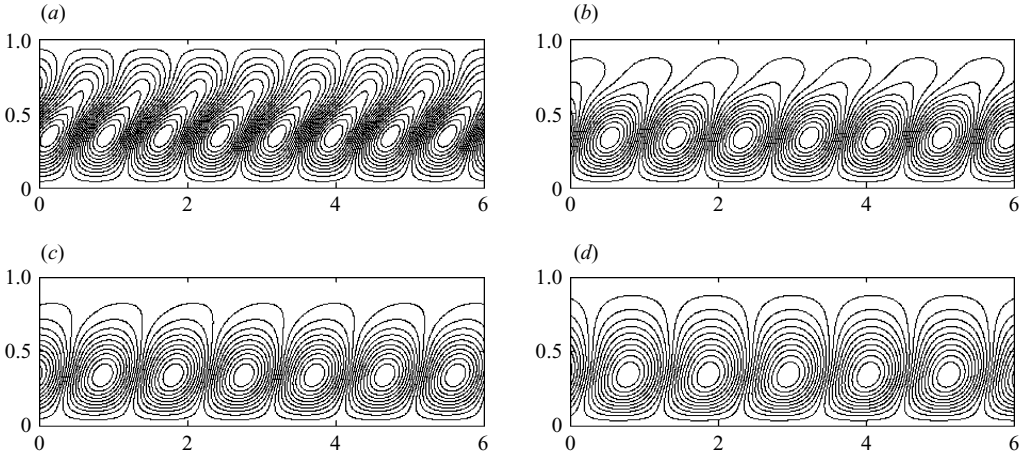


FIGURE 12. Convection cell patterns of the transverse mode for four typical critical states with $Sc_e = 1000$ and $Re = 1$: (a) $\Delta\sigma/\sigma_0 = 1$, $\alpha_x = 4.13$, $Q_c = 4.512 \times 10^4$, $(s_r, s_i) = (0, -4.215)$; (b) $\Delta\sigma/\sigma_0 = 3$, $\alpha_x = 3.58$, $Q_c = 2.597 \times 10^4$, $(s_r, s_i) = (0, -3.518)$; (c) $\Delta\sigma/\sigma_0 = 5$, $\alpha_x = 3.31$, $Q_c = 2.806 \times 10^4$, $(s_r, s_i) = (0, -3.227)$; (d) $\Delta\sigma/\sigma_0 = 10$, $\alpha_x = 2.95$, $Q_c = 4.295 \times 10^4$, $(s_r, s_i) = (0, -2.850)$.

with $\Delta\sigma/\sigma_0 = 1, 3, 5$ and 10 , respectively. At $\Delta\sigma/\sigma_0 = 1$ as shown in figure 12(a), the weak shear flow tends to distort the transverse convection cells, especially in the region within the upper half-channel, and the cell pattern almost occupies the whole thickness of the fluid layer. As $\Delta\sigma/\sigma_0$ increases to 3, the interaction between the dielectrophoretic, diffusive and shear effects seems to constrain the convection cells within the lower half-channel, while the weak convective motion in the upper half-channel still appears to be distorted as shown in figure 12(b). If $\Delta\sigma/\sigma_0$ increases further as shown in figures 12(c) and 12(d), the gradually distinct enhancement of diffusive effect stabilizes the fluid layer with respect to the transverse mode, and the distortion of cell patterns also reduces gradually.

Figure 13(a) reveals the effect of the electric Schmidt number on the instability of the transverse mode, and the corresponding oscillatory frequency of the neutral curves is shown in figure 13(b). Unlike the results in the case of the longitudinal mode that the flow instability is almost independent of the variation of Sc_e , here we find that the transverse mode depends heavily on the electric Schmidt number, and in the present case with $Re = 1$ and $\Delta\sigma/\sigma_0 = 10$, the fluid layer seems to be stabilized monotonically with increasing Sc_e . Since the neutral curve rises rapidly with Sc_e , it is expected that the transverse mode will be replaced by the longitudinal mode as the critical mode, as the electric Schmidt number is high enough. Four typical patterns of convection cells at the critical states are illustrated in figures 14(a)–14(d) for $Sc_e = 10^2, 10^3, 10^4$ and 10^5 , respectively. As seen in these figures, the inclined angle of the convection cell will gradually decrease with higher Sc_e . But when Sc_e is greater than 10^3 , the variation of the cell patterns appears to be limited. The convection is mainly within the lower half-channel and is relatively weak in the region close to the upper plate.

The variations of Q_c and $|s_i|_c$ with Re are respectively demonstrated in figures 15(a) and 15(b) for the transverse mode with three typical values of Sc_e . Curve 1 corresponds to the case we considered in figure 9. For comparison, the corresponding results of longitudinal modes are given in these figures in the form of dashed lines.

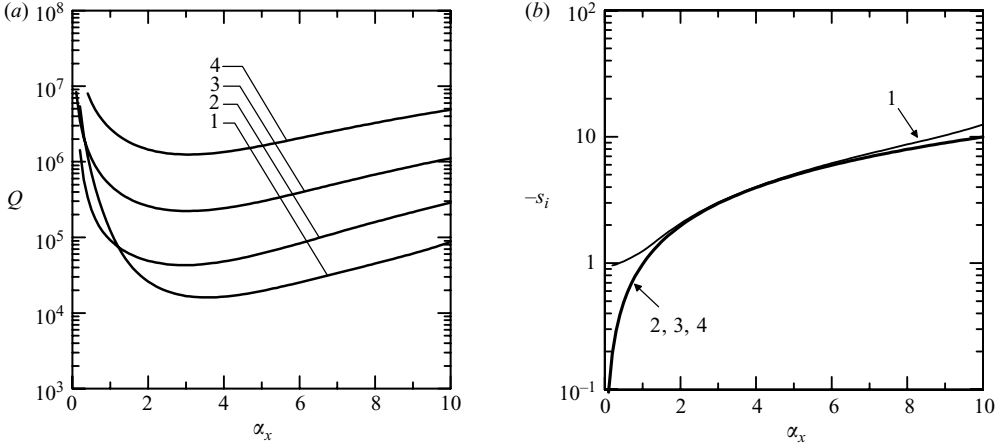


FIGURE 13. (a) The neutral curves and (b) the corresponding oscillatory frequency ($-s_i$) of the transverse mode at $Re = 1$ and $\Delta\sigma/\sigma_0 = 10$: (1) $Sc_e = 10^2$; (2) $Sc_e = 10^3$; (3) $Sc_e = 10^4$; and (4) $Sc_e = 10^5$.

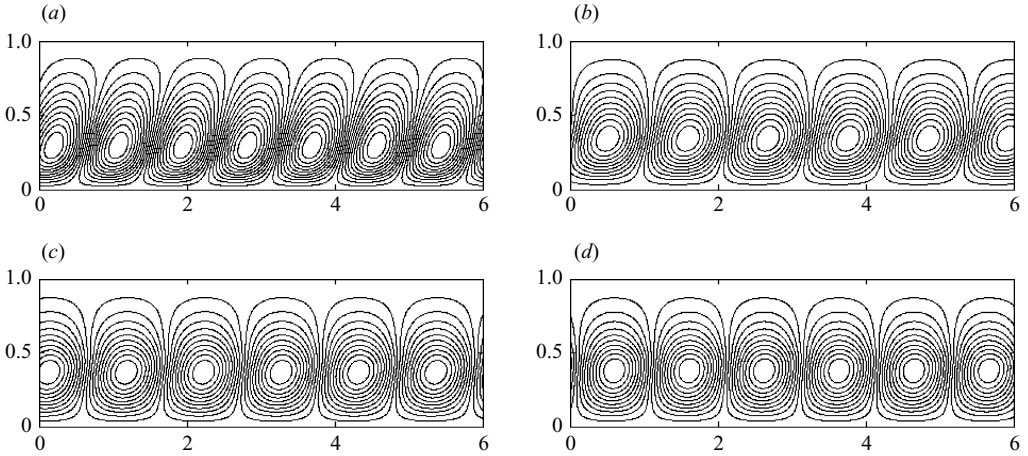


FIGURE 14. Convection cell patterns of the transverse mode for four typical critical states with $Re = 1$ and $\Delta\sigma/\sigma_0 = 10$: (a) $Sc_e = 10^2$, $\alpha_x = 3.55$, $Q_c = 1.605 \times 10^4$, $(s_r, s_i) = (0, -3.562)$; (b) $Sc_e = 10^3$, $\alpha_x = 2.95$, $Q_c = 4.295 \times 10^4$, $(s_r, s_i) = (0, -2.850)$; (c) $Sc_e = 10^4$, $\alpha_x = 3.04$, $Q_c = 2.231 \times 10^5$, $(s_r, s_i) = (0, -3.003)$; (d) $Sc_e = 10^5$, $\alpha_x = 3.16$, $Q_c = 1.217 \times 10^6$, $(s_r, s_i) = (0, -3.147)$.

One can see that as the Reynolds number approaches zero, the transverse mode tends to have the same instability as the longitudinal mode in any case, since the fluid layer gradually becomes quiescent. As Re increases, the variational process of Q_c is the same in each case: decreases with Re , passes a minimum and then increases eventually over Q_c of the longitudinal mode. It is obvious that for a higher value of Sc_e , Q_c will decrease and pass the minimum earlier, making the transverse mode prevail in a smaller range of Re . The results in figure 15(b) show that the oscillatory frequency of the transverse mode increases quickly as Re approaches zero, which indicates the speed of transverse travelling wave will increase dramatically as the onset of the transverse mode will occur in weak shear flow regime. The curves 4–6

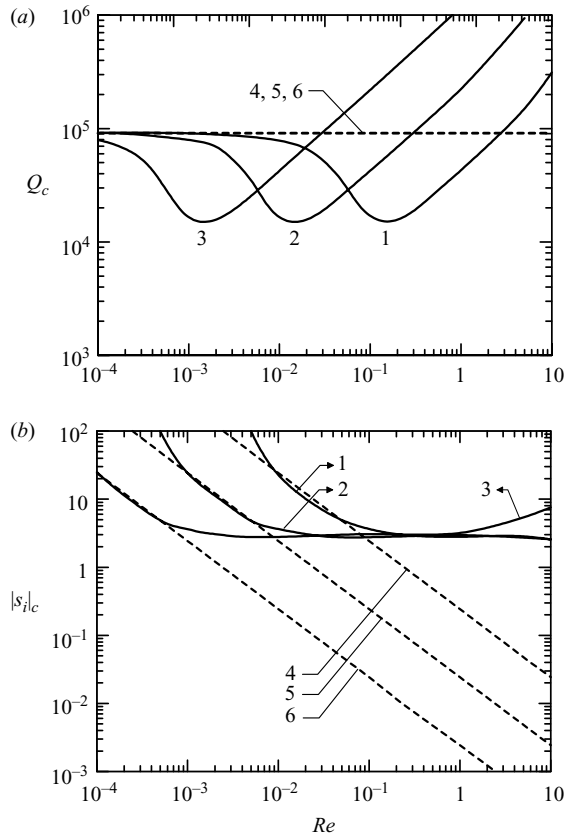


FIGURE 15. The variations of (a) Q_c and (b) $|s_i|_c$ with Re for the transverse mode at $\Delta\sigma/\sigma_0 = 10$ with three typical values of Sc_e : (1) $Sc_e = 10^3$; (2) $Sc_e = 10^4$; and (3) $Sc_e = 10^5$. The corresponding results of the longitudinal mode are given here as dashed lines for comparison: (4) $Sc_e = 10^3$; (5) $Sc_e = 10^4$; and (6) $Sc_e = 10^5$.

for the longitudinal mode appear to be straight lines, showing the magnitude of the critical oscillatory frequency is inversely proportional to the Reynolds number in each case of Sc_e .

Similarly, the variations of Q_c and $|s_i|_c$ with Sc_e can be determined for the assigned values of Re . It is found that the corresponding variational processes are similar to the results shown in figures 15(a) and 15(b), which indicates that the electric Schmidt number exerts a similar effect as the Reynolds number on this electrohydrodynamic flow system. Accordingly, we further examine the variations of Q_c and $|s_i|_c$ with respect to the product of Sc_e and Re as displayed in figures 16(a) and 16(b). Evidently, the instability characteristics can be expressed in a simple form, and the effects of Re and Sc_e both can be inferred from this figure. For the longitudinal modes, the critical value of Q_c is independent of $Sc_e Re$ and $|s_i|_c$ is inversely proportional to this parameter. Note that $Sc_e Re$ is equal to $v_0 d / K_{eff}$ which denotes physically the ratio of convective transport effect to diffusive transport effect. Therefore, the instability behaviours of transverse modes can be described simply by the ratio of these two dominant mechanisms. As shown in figure 16(a), the three assigned typical cases for the transverse mode are almost overlapped in the region under the horizontal dashed line of the longitudinal mode. The corresponding variations of $|s_i|_c$ with $Sc_e Re$ for

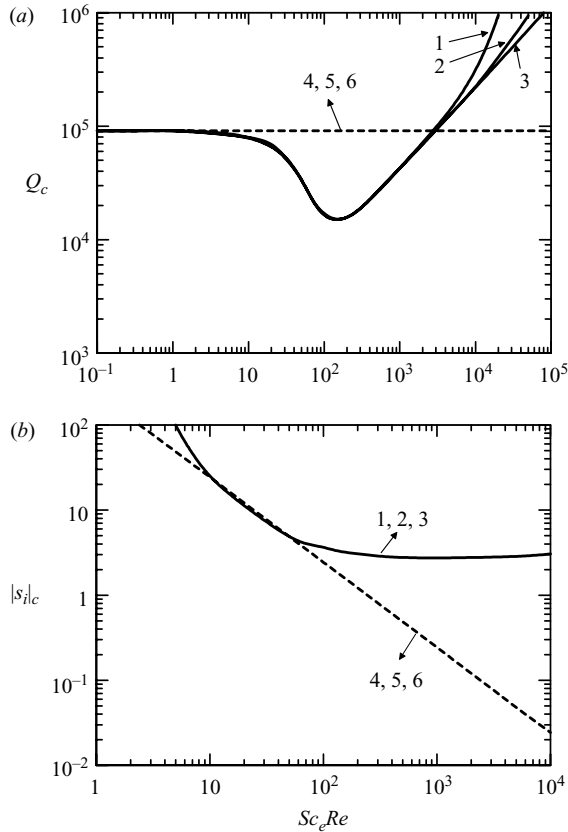


FIGURE 16. The variations of (a) Q_c and (b) $|s_i|_c$ with $Sc_e Re$ at $\Delta\sigma/\sigma_0 = 10$ for both transverse and longitudinal modes with three typical values of Sc_e . The solid lines are the results of the transverse mode: (1) $Sc_e = 10^3$; (2) $Sc_e = 10^4$; (3) $Sc_e = 10^5$. The dashed lines are for the longitudinal mode: (4) $Sc_e = 10^3$; (5) $Sc_e = 10^4$; (6) $Sc_e = 10^5$.

these cases are also the same as shown in figure 16(b), and the value of $|s_i|_c$ tends to be a constant with increasing $Sc_e Re$. Similar results can be observed for any assigned conductivity gradient across the fluid layer.

The variations of Q_c and $|s_i|_c$ with $\Delta\sigma/\sigma_0$ are respectively shown in figures 17(a) and 17(b) for several typical cases of Re . Curve 2 in these figures corresponds to the case we considered in figure 11. The dashed and solid lines of the longitudinal mode represent the oscillatory and the stationary mode, respectively. The results show that if the strength of imposed shear flow is sufficiently large, for example in the case with $Re = 15$, the curve of the transverse mode lies totally above the curve of the longitudinal mode, meaning the transverse mode never becomes critical. On the other hand, if the strength of shear flow is low enough, the transverse mode is possible to give a lower value of Q_c than the longitudinal mode when the conductivity gradient is small enough. The range of $\Delta\sigma/\sigma_0$ in which the transverse mode is dominant extends gradually with decreasing Re . In the region with high value of $\Delta\sigma/\sigma_0$, however, the interaction between the conductivity gradient and the shear flow exerts a strong stabilizing effect on the transverse mode and thus causes the stationary longitudinal mode to always prevail under such a condition. Figure 17(b) illustrates that the value of $|s_i|_c$ of transverse modes generally decreases slightly with $\Delta\sigma/\sigma_0$ in the region in

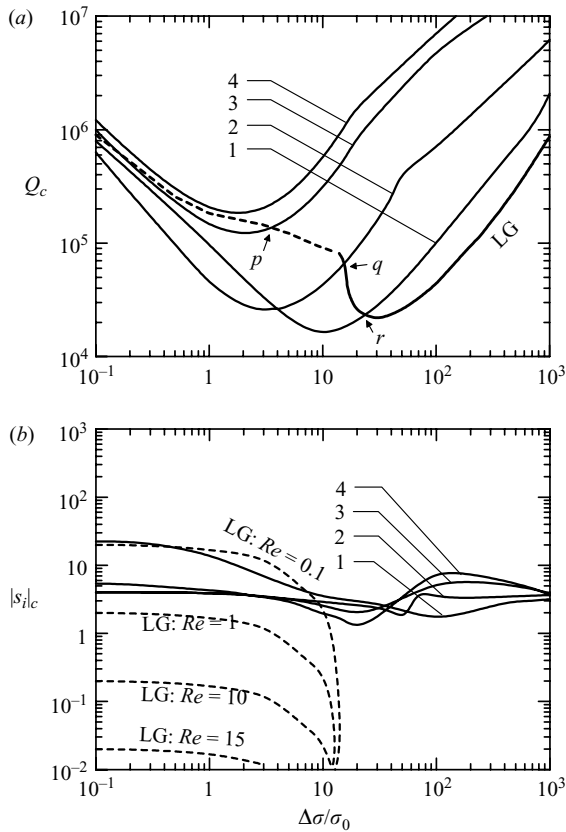


FIGURE 17. The variations of (a) Q_c and (b) $|s_i|_c$ with conductivity gradient $\Delta\sigma/\sigma_0$ for the transverse mode at $Sc_e = 1000$ with four typical values of Re : (1) $Re = 0.1$; (2) $Re = 1$; (3) $Re = 10$; and (4) $Re = 15$. The shift of critical mode between the transverse and longitudinal modes occurs at points p , q and r , which correspond to $\Delta\sigma/\sigma_0 = 3.3$, 15 and 23 , respectively. The corresponding results of the longitudinal mode (LG) are given here for comparison.

which the transverse mode is determinant, whereas the longitudinal mode in each case has an abrupt jump of $|s_i|_c$ occurring at $\Delta\sigma/\sigma_0 = 14.9$ from a finite value to zero, which is caused by the shift of critical mode from the oscillatory to the stationary mode.

4. Conclusions

In this study we have performed a complete linear stability analysis for the electrohydrodynamic flow in a liquid layer between two parallel plates with spatial electrical conductivity gradient. An external electric field is applied over the depth of the fluid layer, and a weak pressure-driven shear flow is subject to the layer in the horizontal direction. In the absence of shear flow, an oscillatory mode is discovered to be dominant in the range of small conductivity gradient. This finding modifies the previous theoretical results based on the assumption of exchange of stabilities and provides a thorough understanding of the linear instability behaviour in this electrohydrodynamic flow system. In the presence of shear flow, both the longitudinal and transverse modes are considered, and the instability of the longitudinal mode is

found to be invariable with respect to the superimposed weak shear flow. However, in contrast to the longitudinal mode, the instability behaviours of the transverse mode are found to profoundly depend on the imposed shear flow. In general, under the conditions with small Reynolds number and low conductivity gradient, the transverse mode exhibits higher instability and becomes the critical mode dominating the onset of instability, while if the Reynolds number or conductivity gradient is large enough, the critical mode shifts to the longitudinal mode. The present results suggest that an imposed weak shear flow may enhance the system instability. Such an instability characteristic is important in the application of mixing or separation of liquid streams, especially in microfluidic devices. Further studies for the instability of electrokinetic flow coupled with the shear flow effect will benefit the design and utilization of microfluidic mixer and separator.

REFERENCES

- BAYGENTS, J. C. & BALDESSARI, F. 1998 Electrohydrodynamic instability in a thin fluid layer with an electrical conductivity gradient. *Phys. Fluids* **10**, 301–311.
- CARRIERE, P. & MONKEWITZ, P. A. 1999 Convective versus absolute instability in mixed Rayleigh–Bénard–Poiseuille convection. *J. Fluid Mech.* **384**, 243–262.
- CHEN, C. H., LIN, H., LELE, S. K. & SANTIAGO, J. G. 2005 Convective and absolute electrokinetic instability with conductivity gradients. *J. Fluid Mech.* **524**, 263–303.
- CLEVER, R. M. & BUSSE, F. H. 1992 Three-dimensional convection in a horizontal fluid layer subjected to a constant shear. *J. Fluid Mech.* **234**, 511–527.
- GAGE, K. S. & REID, W. H. 1968 The stability of thermally stratified plane Poiseuille flow. *J. Fluid Mech.* **33**, 21–32.
- HOBURG, J. F. 1977 Internal electrohydrodynamic instability of liquids with collinear field and conductivity gradients. *J. Fluid Mech.* **84**, 291–303.
- HOBURG, J. F. & MELCHER, J. R. 1976 Internal electrohydrodynamic instability and mixing of fluids with orthogonal field and conductivity gradients. *J. Fluid Mech.* **73**, 333–351.
- HOBURG, J. F. & MELCHER, J. R. 1977 Electrohydrodynamic mixing and instability induced by co-linear fields and conductivity gradients. *Phys. Fluids* **20**, 903–911.
- LI, F., OZEN, O., AUBRY, N., PAPAGEORGIOU, D. T. & PETROPOULOS, P. G. 2007 Linear stability of a two-fluid interface for electrohydrodynamic mixing in a channel. *J. Fluid Mech.* **583**, 347–377.
- LIN, H., STOREY, D. B., ODDY, M. H., CHEN, C. H. & SANTIAGO, J. G. 2004 Instability of electrokinetic microchannel flows with conductivity gradients. *Phys. Fluids* **16**, 1922–1935.
- MELCHER, J. R. 1973 Electrohydrodynamics. In *Proceedings of the IUTAM 13th International Congress of Theoretical and Applied Mechanics* (ed. E. Becker & G. K. Mikhailov) pp. 240–263. Springer.
- MELCHER, J. R. & FIREBAUGH, M. S. 1967 travelling-wave bulk electroconvection induced across a temperature gradient. *Phys. Fluids* **10**, 1178–1185.
- MELCHER, J. R. & TAYLOR, G. I. 1969 Electrohydrodynamics: a review of the role of interfacial shear stresses. *Annu. Rev. Fluid Mech.* **1**, 111–146.
- MICHAEL, D. H. & O'NEILL, M. E. 1970 Electrohydrodynamic instability in plane layers of fluid. *J. Fluid Mech.* **41**, 571–580.
- MOSHER, R. A., SAVILLE, D. A. & THORMANN, W. 1992 *The Dynamics of Electrophoresis*. VCH.
- ODDY, M. H. & SANTIAGO, J. G. 2005 Multiple-species model for electrokinetic instability. *Phys. Fluids* **17**, 064108.
- STONE, H. A., STROOCK, A. D. & AJDARI, A. 2004 Engineering flows in small devices: microfluidics toward a lab-on-a-chip. *Annu. Rev. Fluid Mech.* **36**, 381–411.
- STOREY, B. D. 2005 Direct numerical simulation of electrohydrodynamic flow instabilities in microchannels. *Physica D* **211**, 151–167.
- STOREY, B. D., TILLEY, B. S., LIN, H. & SANTIAGO, J. G. 2005 Electrokinetic instabilities in thin microchannels. *Phys. Fluids* **17**, 018103.
- TARDU, S. 2004 Interfacial electrokinetic effect on the microchannel flow linear stability. *Trans. ASME J. Fluids Engng* **126**, 10–13.

- TAYLOR, G. I. & MCEWAN, A. D. 1965 The stability of a horizontal fluid interface in a vertical electric field. *J. Fluid Mech.* **22**, 1–15.
- THAKAR, R. M. & KUMARAN, V. 2005 Electrohydrodynamic instability of the interface between two fluids confined in a channel. *Phys. Fluids* **17**, 084104.
- THORMANN, W., MOSHER, R. A. & BIER, M. 1986 Experimental and theoretical dynamics of isoelectric focusing. *J. Chromatogr.* **351**, 17.
- TURNBULL, R. J. & MELCHER, J. R. 1969 Electrohydrodynamic Rayleigh–Taylor bulk instability. *Phys. Fluids* **12**, 1160–1166.